

# A giant radio halo in the cool core cluster CL1821+643

A. Bonafede,<sup>1\*</sup> H.T. Intema<sup>2</sup>, M. Brüggen<sup>1</sup>, H. R. Russell<sup>4</sup>, G. Ogrean<sup>1</sup>, K. Basu<sup>3</sup>,  
M. Sommer<sup>3</sup>, R.J. van Weeren<sup>5</sup>, R. Cassano<sup>6</sup>, A. C. Fabian<sup>4</sup>, and H. J. A. Röttgering<sup>7</sup>.

<sup>1</sup> *Hamburger Sternwarte, Universität Hamburg, Gojenbergsweg 112, 21029, Hamburg, Germany.*

<sup>2</sup> *National Radio Astronomy Observatory, 1003 Lopezville Road, Socorro, NM 87801-0387, USA.*

<sup>3</sup> *Argelander Institut für Astronomie, Universität Bonn, D-53121 Bonn, Germany.*

<sup>4</sup> *Institute of Astronomy, Madingley Road, Cambridge CB3 0HA.*

<sup>5</sup> *Harvard-Smithsonian Center for Astrophysics, 60 Garden Street, Cambridge, MA 02138, USA.*

<sup>6</sup> *Istituto di Radioastronomia INAF, via P. Gobetti 101, 40129 Bologna, Italy.*

<sup>7</sup> *Leiden Observatory, Leiden University, 2300 RA Leiden, the Netherlands.*

Accepted Received...

## ABSTRACT

Giant radio halos are Mpc-size sources found in some merging galaxy clusters. The synchrotron emitting electrons are thought to be (re)accelerated by plasma turbulence induced by the merging of two massive clusters. Cool core galaxy clusters have a low temperature core, likely an indication that a major merger has not recently occurred. CL1821+643 is one of the strongest cool core clusters known so far. Surprisingly, we detect a giant radio halo with a largest linear size of  $\sim 1.1$  Mpc. We discuss the radio and X-ray properties of the cluster in the framework of the proposed models for giant radio halos. If a merger is causing the radio emission, despite the presence of a cool-core, we suggest that it should be off-axis, or in an early phase, or a minor one.

**Key words:** galaxy clusters; radio; galaxy clusters: individual: CL1821+643, PSZ1 G094.00+27.41; non-thermal emission; radio observations

## 1 INTRODUCTION

Giant radio halos are extended synchrotron sources found in a fraction of massive galaxy clusters. Their surface brightness is faint ( $\sim 1\mu\text{Jy}/\text{arcsec}^2$  at 1.4 GHz) and characterised by a steep spectrum<sup>1</sup> with a spectral index  $\alpha > 1$  (see Feretti et al. 2012 for a recent review). Radio emission on Mpc-scales requires that the emitting electrons are either (re)accelerated in situ, e.g. through merger-generated turbulence, or continuously injected into the intra-cluster medium (ICM), for instance by inelastic hadronic collisions between relativistic and thermal protons (see review by Brunetti & Jones 2014, and ref. therein). Hadronic models are currently disfavoured as they fail to reproduce the steepest spectrum radio halos, and predict  $\gamma$ -ray emission that has not been observed by the *Fermi* Satellite (e.g. Brunetti et al. 2012). At the same time, recent LOFAR observations of Abell 2256 indicate that the formation process of halos might be more complex than previously thought (van Weeren et al. 2012).

Mini halos are another class of radio sources that are located in cool core galaxy clusters. Their emission is lim-

ited to smaller spatial scales ( $\sim 50$ –500 kpc), and has a steep spectrum (see Feretti et al. 2012, and ref. therein.). Again, the radio emission could be caused by turbulence induced by gas-sloshing in the central potential well or by inelastic collisions between relativistic and thermal protons (e.g. Brunetti & Jones 2014, and references therein).

The picture that emerges from X-ray observations is that mergers between clusters are able to destroy the cool core and leave clear signatures in the emission of the gas (e.g. Rossetti & Molendi 2010). Hence, mergers would be responsible for the cool core non-cool core dichotomy, supporting an evolutionary scenario between cool core and non-cool core clusters (Rossetti et al. 2011). However, simulations show that disrupting the cool core during cluster mergers is not obvious (see e.g. Poole et al. 2008).

Since their first discovery, giant radio halos have always been found in merging galaxy clusters, characterised by the absence of a cool core, while mini halos are found in clusters hosting a cool core (Feretti et al. 2012, and ref. therein).

The cluster CL1821+643 surrounds the quasar H1821+643. CL1821+643 was discovered by Schneider et al. (1992) through optical observations. The redshift information, available for six member galaxies plus the quasar, allowed them to estimate the cluster redshift:  $z=0.299$ . CL1821+643 was also detected by the *Planck* satel-

\* E-mail: annalisa.bonafede@hs.uni-hamburg.de

<sup>1</sup> The radio spectrum is defined as  $S(\nu) \propto \nu^{-\alpha}$ .

**Table 2.** Properties of the giant radio halo.

Frequency MHz	Flux density mJy	LAS "	LLS kpc
323	62±4	250	1100
1665	11.9±0.5	210	930

lite (PSZ1 G094.00+27.41). Through the thermal Sunyaev Zel'dovich (SZ) effect, Planck Collaboration et al. (2013) infer a mass  $M_{500} = 6.311 \times 10^{14} M_{\odot}$ . Russell et al. (2010) observed the cluster with *Chandra*. Thanks to an accurate modelling of the quasar emission, they were able to separate the cluster and quasar emission, and analysed both the ICM properties down to the inner regions, and the interaction of the cluster with the powerful quasar. They found that the temperature of the cluster decreases from  $\sim 9$  keV to 1.3 keV in the centre, and derived a short radiative cooling time of  $\sim 1$  Gyr, typical of strong cool core systems. In the inner 100 kpc, the X-ray morphology shows extended spurs of emission from the core, a small radio cavity, and a weak shock or cold front at  $15''$  from the cluster centre. The optical quasar hosts a FRI radio source, which is not clearly related to the X-ray gas morphology (Russell et al. 2010).

Wold et al. (2002) have analysed the weak lensing properties of the cluster, finding that the cluster is slightly elongated towards North-West, as also suggested by the X-ray emission on large scales (Russell et al. 2010).

In this work, we present new radio observations of CL1821+643, where we discover diffuse radio emission on Mpc scales. In Sec. 2, we present Giant Meterwave Radio Telescope (GMRT) and archival Very Large Array (VLA) observations of the cluster. Results are presented in Sec. 3, where we also analyse the dynamical status of the cluster. We discuss the results and conclude in Sec. 4. Throughout this Letter, we assume a  $\Lambda$ CDM cosmology ( $H_0 = 71 \text{ km s}^{-1} \text{ Mpc}^{-1}$ ,  $\Omega_m = 0.27$ ,  $\Omega_{\Lambda} = 0.73$ ). At the cluster redshift ( $z=0.299$ ) one arc minute corresponds to 265 kpc.

## 2 RADIO OBSERVATIONS

We have observed the cluster CL1821+643 with the GMRT in the framework of a larger project aimed at discovering diffuse emission in clusters detected by *Planck*. Observations were carried out at 323 MHz, using a 33 MHz bandwidth subdivided into 256 channels and 8s integration time. The sources 3C48 and 3C286 were observed for 15 minutes at the beginning of the observing block, and used as absolute flux and bandpass calibrators, adopting the Scaife & Heald (2012) absolute flux scale. The absolute flux calibrators were also used to estimate the instrumental contribution to the antenna gains, which is also needed for ionospheric calibration, and the instrumental phase information was used to correct the target field. The main steps of the calibration procedure are outlined below, and are based on AIPS (NRAO Astronomical Image Processing System), SPAM (Intema et al. 2009) and Obit (Cotton 2008) tools. Strong Radio Frequency Interferences (RFIs) were removed from the target field data by statistical outlier flagging tools. Remaining low-level RFIs were modelled and subtracted from the data using Obit. The dataset has been averaged down to

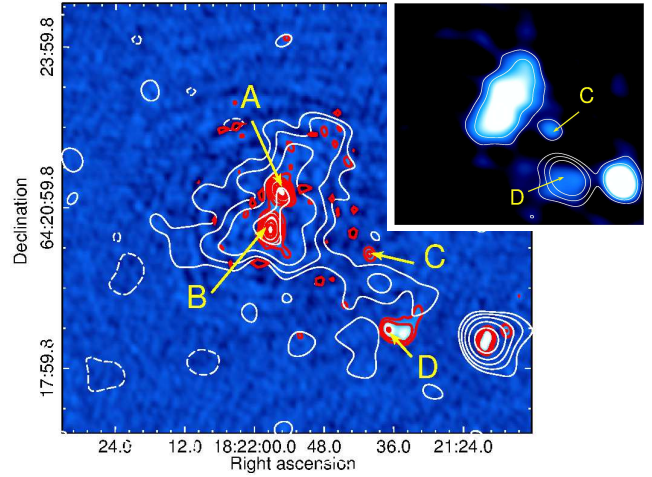


**Figure 1.** The cluster CL1821+643. Main panel colors and red contours: HR image at 323 MHz. White contours: LR image at 323 MHz. The first contours are drawn at  $3\sigma_{\text{LR,HR}}$ , other contours are spaced by a factor 2. The  $-3\sigma_{\text{LR,HR}}$  contours are dashed. In the inset: LR image at 1665 MHz in colours and contours (at  $3, 6, 12 \sigma_{\text{LR}}$ , the  $-3\sigma_{\text{LR}}$  contour is dashed). The inset shows the same region as the main panel (A and B have been subtracted).

24 channels, a compromise to speed up the imaging process and avoid significant bandwidth smearing. For the phase calibration, we started from a model derived from the northern VLA Sky Survey (NVSS, Condon et al. 1998) and then proceeded with self-calibration loops. To compensate for the non-coplanarity of the array, we used the polyhedron (facet-based) wide-field imaging technique as available in AIPS. We performed several rounds of imaging and self-calibration, inspecting the residual visibilities for a more accurate removal of low-level RFIs. To correct for ionospheric effects, we applied SPAM calibration and imaging. The presence of strong sources in the field of view enables one to derive directional-dependent gains for each of them and to use these gains to fit a time variable phase-screen over the entire array. After ionospheric corrections, data has been imported to CASA (Common Astronomy Software Applications package) for further imaging and self-calibration steps.

In addition, we have downloaded an observation performed in the L band in the D array configuration from the VLA data archive. Using AIPS, we followed a standard procedure for the data reduction. The source 3C286 has been used to set the absolute flux, using the Perley & Taylor (1999) flux scale. As no phase-calibrator was scheduled during the observation, we transferred the gains from 3C286 to the target and proceeded with cycles of self-calibration on the target field. Details about the observation are listed in Table 1.

For both GMRT and VLA observations, we have produced three different images of the target field:

- Full-resolution image (FR): using all the baselines and Briggs weighting scheme with robust  $R = 0$ .
- High-resolution image (HR): using all the baselines longer than  $0.9 \text{ k}\lambda$ , to filter out the emission on scales larger than 1 Mpc. Sources have been cleaned down to  $1\sigma$ ,  $\sigma$  being the rms noise level of the image. On these images, we have identified the sources within a radius of 1 Mpc from the cluster centre (see Fig. 1). The quasar and the head-tail radio galaxy de-

**Table 1.** Radio observations of CL1821+643.

Pointing RA & DEC J2000	Obs. date	$\nu$ MHz	$\Delta\nu$ MHz	t h	$\theta_{\text{FR}}$ "×"	$\sigma_{\text{FR}}$ mJy/beam	$\theta_{\text{HR}}$ "×"	$\sigma_{\text{HR}}$ mJy/beam	$\theta_{\text{LR}}$ "×"	$\sigma_{\text{LR}}$ mJy/beam
18 21 57.3 +64 20 36	27-01-2013	323	33	6	12 × 9	0.07	11 × 7	0.13	30×26	0.20
18 21 57.2 +64 20 36	22-09-1996	1665	50	0.37	49 × 32	0.10	45 × 30	0.16	53×38	0.20

Col. 1: Right ascension and declination of the pointing centre if the observation; Col. 2: Date of observation;

Col. 3: Central frequency ; Col. 4: Bandwidth; Col 5: Net on-source time; Col 6: Restoring beam of the full-resolution image;

Col 7: rms noise of the full resolution image. Col. 8: Restoring beam of the high-resolution image; Col 9: rms noise of the high-resolution image.

Col 10: Restoring beam of the low-resolution image. Col. 11: rms noise of the low-resolution image

ected by Blundell & Rawlings (2001) are labelled as B and A, respectively.

• Low-resolution image (LR): First, we subtracted from the uv-data the visibilities corresponding to the the clean components of the HR image for the sources A, B, C, and D (see Fig. 1). Then, we imaged the uv-subtracted dataset including all baselines and tapering down the baselines longer than  $4k\lambda$  to gain sensitivity towards the diffuse emission.

The final images were corrected for the primary beam response. Furthermore, GMRT images have been corrected for the system temperature using the Haslam et al. (1995) all-sky map. We estimate that the residual amplitude errors are of the order of 6% at 323 MHz. VLA observations amplitude errors are  $\sim 4\%$  at 1.665 GHz.

### 3 RESULTS

#### 3.1 Radio emission and cluster properties

As shown in Fig. 2, diffuse radio emission is clearly detected in CL1821+643. We note that other compact sources, that we subtracted from the uv-data, do not leave residuals in the LR images. To analyse its radio morphology we rely on the 323 MHz observation, which has a longer exposure time and a wider range of baselines with respect to the 1.665 GHz one. In Fig. 2 the LR image at 323 MHz is shown. The radio emission is located at the cluster centre, and extends for  $\sim 1$  Mpc towards NW. Because of its size and location, we classify this emission as a giant radio halo.

Further emission is tentatively detected at  $3\sigma$  significance at the west of the cluster (see Fig. 2). Although it does not overlap with sources C and D (Fig. 1), deeper observations would be needed to confirm the detection. We have measured the flux density of the giant radio halo on the LR images at 323 MHz and at 1.665 GHz. The error on the giant radio halo flux has been estimated as  $\Delta S = \sqrt{(F_h \text{Err}_{\text{cal}})^2 + (\sigma_{\text{LR}} \sqrt{N_b})^2}$ , where  $F_h$  is the flux density of the giant radio halo measured from the LR image,  $\text{Err}_{\text{cal}}$  is the calibration error,  $\sigma_{\text{LR}}$  is the rms noise of the LR image, and  $N_b$  is the number of independent beams sampling the diffuse emission. Details about the giant radio halo flux density and size are listed in Table 2.

To estimate the spectral index of the halo, we imaged the uv-subtracted data, selecting the range of baselines that are densely sampled by both observations (from  $0.3k\lambda$  to  $5.5k\lambda$ ) and convolved the images with the same beam of  $\sim 60'' \times 50''$ . Because of the poorer sensitivity of the 1.665 GHz observation, only the central region is detected. It has a spectral index of  $\alpha = 0.87 \pm 0.04$ . Using these images, a lower limit for the spectral index of the entire halo can be

derived, computing the flux densities in both images wherever the 323 MHz image has a signal above 3 times the noise level, obtaining  $\alpha \geq 1.04$ . Using the fluxes measured in the LR images at 323 MHz and 1.665 GHz (Table 2), we obtain an upper limit for the spectral index:  $\alpha \leq 1.1$ .

The power of giant radio halos is known to correlate with the cluster X-ray luminosity:  $P_{1.4 \text{ GHz}} - L_{[0.1-2.4] \text{ keV}}$  correlation, and with the cluster SZ signal:  $\text{SZ} - P_{1.4 \text{ GHz}}$  correlation (Basu 2012, Cassano et al. 2013). We have computed the power of the giant radio halo at 1.4 GHz extrapolating the flux density observed in the 323 MHz image and assuming a spectral index in the range  $1.04 \leq \alpha \leq 1.1$ . The estimated power at 1.4 GHz,  $P_{1.4 \text{ GHz}}$ , is in the range  $(3.6 - 3.8) \times 10^{24} \text{ W Hz}^{-1}$ . We have computed  $L_{[0.1-2.4] \text{ keV}}$  from the *Chandra* observation of the cluster presented in Russell et al. (2010), using an absorbed MEKAL model in the X-ray fitting package *xspec* with a temperature  $T = 7.0 \pm 0.2 \text{ keV}$ , and a metallicity  $Z = (0.29 \pm 0.03) Z_{\odot}$ . We obtain  $L_{[0.1-2.4 \text{ keV}]} = (1.44 \pm 0.01) \times 10^{45} \text{ erg s}^{-1}$ , which would put the halo a factor  $\sim 3$  below the  $P_{1.4 \text{ GHz}} - L_{[0.1-2.4] \text{ keV}}$  correlation, i.e. the cluster is under luminous in radio for its X-ray luminosity.  $L_{[0.1-2.4 \text{ keV}]}$  is here computed within an aperture of 650 kpc, the maximum allowed by this *Chandra* observation, while Cassano et al. (2013) computed  $L_{[0.1-2.4 \text{ keV}]}$  within  $r_{500}$ , corresponding to  $\sim 1.2$  Mpc for this cluster. Hence, the cluster could be more than a factor 3 below the correlation. The SZ flux is a more robust estimate of the cluster mass, since it is less biased by the dynamical state of the cluster. Indeed, the cluster follows the  $\text{SZ} - P_{1.4 \text{ GHz}}$  correlation within the errors.

#### 3.2 Characterisation of the dynamical state

Since radio halos are always found in merging galaxy clusters, it is crucial to characterise the dynamical status of CL1821+643. To this aim, we compute three dynamical indicators, extensively used in the literature (e.g. Böhringer et al. 2010): the power ratio  $P_3/P_0$ , the centroid shift,  $w$ , and the concentration parameter,  $c$ . Recently, Cassano et al. (2010) have used these methods, finding that clusters with and without radio halos occupy different regions in the morphological diagrams (see Fig. 3), and confirming that radio halos are always associated to merging clusters.

The *Chandra* image of the cluster CL1821+643 has been exposure, vignetting, and background corrected, and the quasar emission has been subtracted.  $P_3/P_0$ ,  $w$ , and  $c$  have been computed within an aperture radius  $R_{\text{ap}} = 500$  kpc. Because of the quasar and of the readout-strip, the centre of the cluster, used in the following analysis, is not

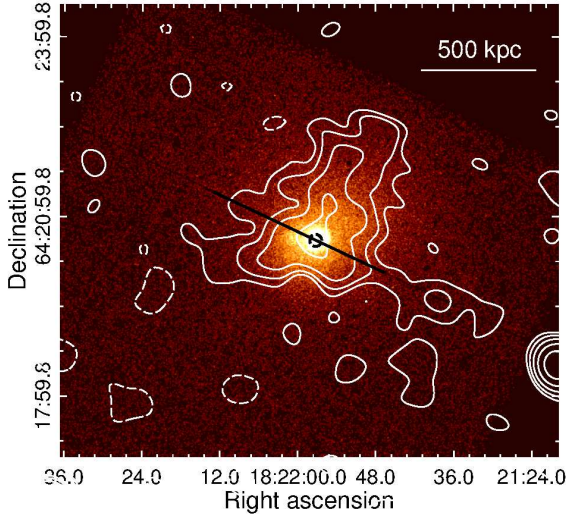


**Figure 2.** Colors: *Chandra* exposure-corrected image in the 0.5 - 7 keV energy band smoothed with a 2D Gaussian of  $\sigma = 1''$ . The readout-strip is blanked. Contours are the same as the 323 MHz LR image in Fig. 1. The black dashed circle is centred on the quasar and has a radius of  $0.05 \times R_{ap}$  (see text for details).

uniquely defined. We consider as centre the position of the quasar.<sup>2</sup> The errors and the photon bias have been estimated through Monte-Carlo simulations, following the approach of Böhringer et al. (2010).

The power ratio is a multipole decomposition of the two-dimensional projected mass distribution (Buote & Tsai 1995). We have determined the power ratio  $P_3/P_0$ , the lowest power ratio moment providing a clear substructure measure, obtaining  $P_3/P_0 = (5.8 \pm 1.4) \times 10^{-8}$ . Since the momenta are computed excising the inner  $0.05 \times R_{ap}$ , the quasar does not affect the  $P_3/P_0$  computation.

The centroid shift method (Maughan et al. 2008) measures the standard deviation of the projected separation between the X-ray peak and the centroid in units of  $R_{ap}$ , computed within circles of increasing radius (from  $0.05 \times R_{ap}$  to  $R_{ap}$ , in steps of  $0.05 \times R_{ap}$ ). The centroid shift,  $w$ , has been computed minimising the  $P_1$  dipole within circles of increasing radius (as done by Böhringer et al. 2010), and computing the X-ray weighted centroid (following Cassano et al. 2010). We obtain  $w = (5.98 \pm 0.07) \times 10^{-2}$  and  $w = (3.6 \pm 0.07) \times 10^{-2}$ , respectively.

The concentration parameter,  $c$ , measures the ratio between the X-ray surface brightness within 100 kpc over the surface brightness within 500 kpc. Because of the quasar and the readout-strip, we can only derive limits for  $c$ , with and without the quasar subtraction. We obtain  $0.3 < c < 0.4$ . In Fig. 3 we show the position of the cluster in the  $P_3/P_0 - c$ , and  $w - c$  diagrams, taken from Cassano et al. (2010). In the  $P_3/P_0 - c$  diagram, the cluster is among the radio-quiet ones. The  $w$  parameter, instead, has a typical value for clusters with a giant radio halo, i.e. dynamically disturbed. Hence, in

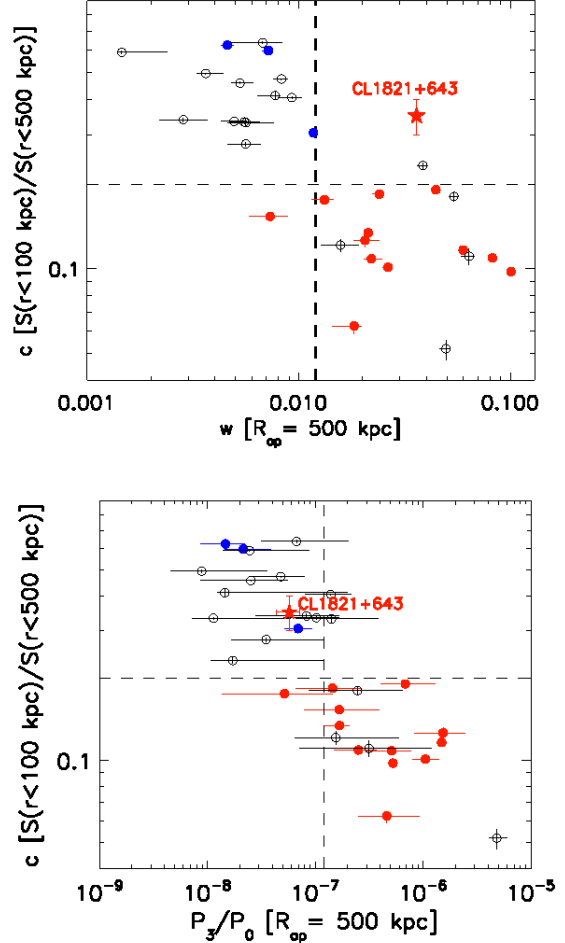


**Figure 3.** The  $c-w$  (top panel) and  $c-P_3/P_0$  (bottom panel) diagrams. The red star marks the position of CL1821+643. Dashed lines are the median of the parameters, which define the radio-loud and radio-quiet quadrants, red dots mark giant radio halos, blue dots mark mini halos, black circles mark radio quiet clusters (points and lines are taken from Cassano et al. 2010).

the  $c-w$  and  $w-P_3/P_0$  diagram (not shown here), the cluster is in a rather empty quadrant.

## 4 DISCUSSION AND CONCLUSIONS

A giant-radio halo in a cool core cluster challenges our understanding of cool core clusters, major mergers, and radio emission. So far, giant radio halos have always been found in massive mergers, and never in cool core clusters, hence supporting the idea that major mergers, necessary to power giant radio halos, also disrupt the cool core. In this framework, few peculiar cases have been found: RXJ1347.5-1145, which shows both a cool core and merging signatures, and hosts a mini halo (Gitti et al. 2007), and A2142, where the cool core has been destroyed by the merger, but some remnants seem to be sloshing, and a giant radio halo has been detected (Farnsworth et al. 2013). CL1821+643 is the only case found so far where a giant radio halo is detected in a cluster that preserves the cool core.

So far, giant radio halos and mini halos have been considered as two separate classes of sources. CL1821+643 could

<sup>2</sup> We repeated the calculations assuming different centres: (i) the pixel that provides the minimum value of the dipole  $P_1$ , (ii) the X-ray centroid, and (iii) the position where the X-ray emission is maximum. All these choices are affected by the quasar excision and, as such, less reliable. Nonetheless, the results we obtain differ by few %.

be witnessing the transition between these two stages: turbulent motions generated during mergers could switch off the mini halo and transport relativistic electrons on larger scales (Brunetti & Jones 2014). In this case, one should assume that a merger is taking place here, and that it has not disrupted the cool core.

The X-ray observations indicate that the cluster is not undergoing a major merger similar to those detected in other clusters with radio halos. However, it could be undergoing a minor or off-axis merger, which may be responsible for the high value of the centroid shift  $w$  and the possible sloshing structure (Russell et al. 2010). As none of the morphological indicators is sensitive to mergers along the line of sight, spectroscopic observations are needed to finally assess the dynamical status of CL1821+643. The analysis of the X-ray substructure highlights the peculiarities of CL1821+643, even without the radio information. Indeed, it shows features typical of systems in dynamical equilibrium (cool core, temperature and entropy drop, high value of the concentration parameter  $c$ ) as well as indication of large-scale perturbations (high value of the centroid shift  $w$  and sloshing).

Another possibility is that the radio emission is not a radio halo but a radio relic seen in projection. Radio relics could be originated by minor off-axis mergers that preserve the cool core, like in Abell 1664 (Govoni et al. 2001). However, the presence of a radio relic seen in projection onto the cluster centre is unlikely (Vazza et al. 2012) and neither the morphology of the emission nor the NW elongation - roughly following the X-ray emission - would favour this interpretation.

Finally, the extended emission could result from the past activity of a FR II radio source, now turned into the FRI associated with the quasar, hence not requiring a merger to accelerate the particles. We regard this possibility as less plausible because of the relatively low  $\alpha$ , and the morphology of the radio emission. However, spectral index maps would be needed to investigate this scenario.

To conclude, our results can be summarised as follows:

- We have analysed the radio emission of the cluster CL1821+643 - also known as PSZ1 G094.00+27.41 - finding for the first time a strong cool core cluster that hosts a giant radio halo, having a largest linear scale of  $\sim 1.1$  Mpc.
- We have constrained the spectral index between 323 MHz and 1.665 GHz to be  $1.04 \leq \alpha \leq 1.1$ , meaning that the halo is in an early stage of its radio-loud phase.
- The radio power at 1.4 GHz is at least a factor  $\sim 3$  below the  $P_{1.4\text{ GHz}} - L_{[0.1-2.4]\text{ keV}}$  correlation, while it sits on the  $SZ - P_{1.4\text{ GHz}}$  correlation.
- An analysis of the cluster, based on the X-ray  $P_3/P_0$  and  $c$  morphological estimators would classify the cluster among the radio-quiet systems. However, the high value of  $w$  indicates that some merger has happened here.

If the radio emission is powered by merger-induced turbulence, we have to assume that the cluster is undergoing a merger which has not disrupted the cool core, but has injected a sufficient amount of energy to power the radio emission. In re-acceleration scenarios, this suggests that a higher fraction of the gravitational energy, released into the ICM during mergers, might be channelled into the (re)acceleration of particles, or that a seed population of energetic particles is already present.

## ACKNOWLEDGMENTS

We thank F. de Gasperin and F. Vazza for useful discussions. A.B. and M.B. acknowledge support by the research group FOR 1254 funded by the Deutsche Forschungsgemeinschaft. H.R. acknowledges support from ERC Advanced Grant Feedback. R.J.W. is supported by NASA through Einstein Postdoctoral grant PF2-130104 (Chandra X-ray Center, SAO for NASA, contract NAS8-03060). We thank the staff of the GMRT. NRAO is a facility of the National Science Foundation operated under Associated Universities Inc.

## REFERENCES

- Basu K., 2012, MNRAS, 421, L112  
 Blundell K. M., Rawlings S., 2001, ApJL, 562, L5  
 Böhringer H. et al., 2010, A&A, 514, A32  
 Brunetti G., Blasi P., Reimer O., Rudnick L., Bonafede A., Brown S., 2012, MNRAS, 426, 956  
 Brunetti G., Jones T. W., 2014, ArXiv e-prints  
 Buote D. A., Tsai J. C., 1995, ApJ, 452, 522  
 Cassano R. et al., 2013, ApJ, 777, 141  
 Cassano R., Ettori S., Giacintucci S., Brunetti G., Markevitch M., Venturi T., Gitti M., 2010, ApJL, 721, L82  
 Condon J. J., Cotton W. D., Greisen E. W., Yin Q. F., Perley R. A., Taylor G. B., Broderick J. J., 1998, AJ, 115, 1693  
 Cotton W. D., 2008, PASP, 120, 439  
 Farnsworth D., Rudnick L., Brown S., Brunetti G., 2013, ApJ, 779, 189  
 Feretti L., Giovannini G., Govoni F., Murgia M., 2012, A&AR  
 Gitti M., Ferrari C., Domainko W., Feretti L., Schindler S., 2007, A&A, 470, L25  
 Govoni F., Feretti L., Giovannini G., Böhringer H., Reiprich T. H., Murgia M., 2001, A&A, 376, 803  
 Haslam C. G. T., Salter C. J., Stoffel H., Wilson W. E., 1995, Astronomy Data Image Library, 1  
 Intema H. T., van der Tol S., Cotton W. D., Cohen A. S., van Bemmelen I. M., Röttgering H. J. A., 2009, A&A, 501, 1185  
 Maughan B. J., Jones C., Forman W., Van Speybroeck L., 2008, APJS, 174, 117  
 Perley R. T., Taylor G. B., 1999, VLA Calibrator Manual, Tech. rep. NRAO  
 Planck Collaboration et al., 2013, ArXiv e-prints  
 Poole G. B., Babul A., McCarthy I. G., Sanderson A. J. R., Fardal M. A., 2008, MNRAS, 391, 1163  
 Rossetti M., Eckert D., Cavalleri B. M., Molendi S., Gastaldello F., Ghizzardi S., 2011, A&A, 532, A123  
 Rossetti M., Molendi S., 2010, A&A, 510, A83+  
 Russell H. R., Fabian A. C., Sanders J. S., Johnstone R. M., Blundell K. M., Brandt W. N., Crawford C. S., 2010, MNRAS, 402, 1561  
 Scaife A. M. M., Heald G. H., 2012, MNRAS, 423, L30  
 Schneider D. P., Bahcall J. N., Gunn J. E., Dressler A., 1992, AJ, 103, 1047  
 van Weeren R. J. et al., 2012, A&A, 543, A43  
 Vazza F., Brügggen M., van Weeren R., Bonafede A., Dolag K., Brunetti G., 2012, MNRAS, 421, 1868

Wold M., Lacy M., Dahle H., Lilje P. B., Ridgway S. E.,  
2002, MNRAS, 335, 1017